Catalysis Science & Technology

PAPER

Inhibitory effect of NO_2 on the selective catalytic reduction of NO_x with NH_3 over one-pot-synthesized Cu–SSZ-13 catalyst†

Cite this: *Catal. Sci. Technol.*, 2014, 4, 1104

Lijuan Xie, Fudong Liu, Kuo Liu, Xiaoyan Shi and Hong He*

Received 13th November 2013,
Accepted 14th January 2014

DOI: 10.1039/c3cy00924f

www.rsc.org/catalysis

The selective catalytic reduction of NO_x with NH_3 (NH_3–SCR) on a Cu–SSZ-13 catalyst prepared by a one-pot-synthesis method was inhibited by NO_2 in the low temperature range. NH_4NO_3 that accumulated on the catalyst surface was the reason for this phenomenon. The key step of the NH_3–SCR reaction over the catalyst at low temperatures was the formation of nitrate on the Cu sites. However, NO_2, with its larger kinetic diameter, could not form nitrate species on the Cu sites efficiently, and part of these molecules formed NH_4NO_3 in combination with NH_4^+ on the Brønsted acid sites. The consumption rate of NH_4NO_3 by NO was lower than its accumulation under "fast SCR" conditions at low temperatures, making the active sites become blocked by NH_4NO_3 and inactive. The results of kinetic studies indicate that N_2 formation mainly results from the reaction between NO and NH_3, even under "fast SCR" reaction conditions.

1. Introduction

Currently, the selective catalytic reduction of NO_x with NH_3 (NH_3–SCR) is one of the most promising technologies for NO_x emission control from diesel engine exhaust. Researchers have conducted many studies to improve the performance of catalysts to meet more and more stringent emission standards, and a great deal of work has been carried out to investigate the active sites and reaction routes of the NH_3–SCR reaction for different catalyst systems as well.[1–5] A complex reaction pathway was observed during the reduction of NO_x with NH_3 in previous studies. The main reactions include standard SCR, fast SCR, NH_4NO_3 formation and N_2O formation. Because the fraction of NO in NO_x is *ca.* 90% in real diesel exhaust, the "standard SCR" reaction (1) is the most important of the four reactions described above.[6]

$$4NH_3 + 4NO + O_2 \rightarrow 4N_2 + 6H_2O \quad (1)$$

The SCR performance is always enhanced greatly when the NO_2 fraction in the feed gas is increased to about 50%; this is known as the "fast SCR" reaction according to the following stoichiometric equation:[7–10]

$$2NH_3 + NO + NO_2 \rightarrow 2N_2 + 3H_2O \quad (2)$$

The oxidation of NO to NO_2 has been proposed to be the rate-limiting step in the NH_3–SCR reaction.[11,12] For this reason, a diesel oxidation catalyst (DOC) is usually put upstream of the SCR catalyst to convert some NO to NO_2 in real applications.[7,13] However, when NO_2 is present in the feed gas, N_2O is often produced at higher levels through the decomposition of NH_4NO_3, which is formed easily by reaction between NH_3 and NO_2. Notably, N_2O is an undesirable by-product in deNO_x reactions due to its greenhouse activity and also its ability to destroy the ozone layer.[1,14–16] Thus, researchers seek to develop catalysts with both excellent NH_3–SCR activity and N_2 selectivity.

Recently, Cu–CHA materials (such as Cu–SSZ-13 and Cu–SAPO-34), a new type of NH_3–SCR catalyst, have shown improved NH_3–SCR activity, N_2 selectivity and hydrothermal stability compared with the existing Cu–zeolite catalysts.[4,5,17–19] Attractively, their small pore structures contribute to a high resistance to small hydrocarbon molecules such as C_3H_6.[20,21] This feature was helpful for their application under real working conditions. The role of NO_2 and the formation of N_2O in the NH_3–SCR reaction catalyzed by Cu–CHA catalysts have also attracted much attention. There was little N_2O observed in the NH_3–SCR reaction over the Cu–SSZ-13 catalyst even when a large amount of NO_2 was present in the feed gas.[22] Zhu *et al.* analyzed the relationship between different NH_3

Research Center for Eco-Environmental Sciences, Chinese Academy of Sciences, 18 Shuangqing Road, Haidian District, Beijing 100085, China
E-mail: honghe@rcees.ac.cn; Fax: +86 10 62849123; Tel: +86 10 62849123

† Electronic supplementary information (ESI) available: NH_3–SCR performance of the $Cu_{3.9}$–SSZ-13 catalyst; reactions between pre-adsorbed species of NH_3 and NO + O_2. See DOI: 10.1039/c3cy00924f

adsorbed species and the formation of N_2 and N_2O based on the results of *in situ* DRIFTS-MS studies over the Cu–SSZ-13 catalyst, suggesting that the formation of N_2O was associated with the reaction of NO_x with proton-adsorbed NH_3 *via* the formation and subsequent thermal decomposition of NH_4NO_3.[23] Kwak *et al.* found that the addition of NO_2 did not significantly increase the rate of NH_3–SCR reaction over the Cu–SSZ-13 catalyst, suggesting that the mechanism over this CHA-based catalyst was different from that observed for other zeolites.[24] In the study, the Cu^+NO^+ species was identified as an important intermediate, which formed in the reaction between Cu^{2+} and NO. Different preparation methods were used to prepare Cu–SSZ-13 catalysts with superior NH_3–SCR performance in previous reports.[25,26] Deka *et al.* prepared Cu–SSZ-13 catalysts *via* chemical vapor deposition and wet chemical routes, suggesting that the mononuclear Cu^{2+} species was preferred for the formation of N_2.[25]

The one-pot-synthesis method is also effective in the preparation of a Cu–SSZ-13 sample using a less expensive copper–amine complex (Cu–TEPA) as a structure-directing agent (SDA).[26] In this method, the cost of the Cu–SSZ-13 catalyst was decreased greatly with the lower-cost SDA and higher Cu loading efficiency. More importantly, the optimal one-pot-synthesized Cu–SSZ-13 catalyst exhibited very good NH_3–SCR activity, especially in the low temperature range. Thus, Cu–SSZ-13 catalysts with excellent NH_3–SCR performance and much lower cost could be obtained *via* this method, which is beneficial for the wide use of Cu–SSZ-13 catalysts. However, there have been few studies on the NH_3–SCR reaction mechanism relative to the one-pot-synthesized Cu–SSZ-13 catalyst. This paper focuses on the effect of NO_2 on the NH_3–SCR reaction catalyzed by Cu–SSZ-13 prepared by the one-pot-synthesis method. Surprisingly, it was found that NO_2 inhibited the NH_3–SCR activity in the low temperature range (<200 °C), which was in contradiction to the promotional effect of NO_2 referred to as "fast SCR".[18,22] The NH_3–SCR performance was tested under different NO_2/NO_x ratios, and the explanations were given based on the results of *in situ* DRIFTS experiments and kinetic studies. The results indicate that increasing the NO_2 ratio directly in the feed gas is not an effective way to improve NH_3–SCR performance of the Cu–SSZ-13 catalyst prepared by the one-pot-synthesis method.

2. Experimental

2.1 Catalyst preparation and activity test

The initial Cu–SSZ-13 catalyst sample was synthesized using the same procedure as in a previous report.[27] Because of the relatively high Cu content in the initial sample, some post-treatments were necessary to obtain catalysts with suitable Cu loadings. Dilute nitric acid solution was also preferred to adjust the Cu loading in the sample instead of NH_4NO_3 solution. In this study, a suspension of the initial Cu–SSZ-13 sample in nitric acid solution with pH = 1 was stirred for 12 h at 80 °C. After filtration, the sample was dried overnight at 120 °C and successively calcined at 600 °C to remove the residual template molecules.

The SCR activity tests of the sieved powder catalysts were carried out in a fixed-bed quartz flow reactor at atmospheric pressure. 50 mg samples of catalysts were used, and the gas hourly space velocity (GHSV) was *ca.* 400 000 h^{-1}. The reaction conditions were controlled as follows: $[NO_x] = [NO] + [NO_2]$ = 500 ppm, 500 ppm NH_3, 5 vol.% O_2, balance N_2. The total flow rate was held at 500 mL min^{-1}. The effluent gas including NO, NH_3, NO_2 and N_2O was continuously analyzed using an online NEXUS 670-FTIR spectrometer equipped with a heated, low volume (0.2 L) multiple-path gas cell (2 m). The FTIR spectra were collected throughout and the results were recorded when the SCR reaction reached a steady state. Then, the NO_x conversion and N_2O concentration were calculated accordingly.

$$NO_x \text{ conversion} = \left(1 - \frac{[NO]_{out} + [NO_2]_{out}}{[NO]_{in} + [NO_2]_{in}}\right) \times 100\%$$

2.2 *In situ* DRIFTS experiments

The *in situ* DRIFTS experiments were performed using an FTIR spectrometer (Nicolet Nexus 670) equipped with a Smart Collector and an MCT/A detector. The reaction temperature was controlled precisely by an Omega programmable temperature controller. Prior to each experiment, the catalyst was pretreated at 550 °C for 20 min in a flow of 20 vol.% O_2/N_2 and then cooled down to 120 °C. The background spectrum was collected in flowing N_2 and automatically subtracted from the sample spectrum. In order to identify the adsorbed species, the catalysts were exposed to a flow of 1000 ppm NH_3/N_2 or 1000 ppm NO (NO_2) + 5 vol.% O_2/N_2 (200 mL min^{-1}) at 120 °C for 0.5 h, followed by a N_2 purge for another 0.5 h. The reaction conditions were controlled as follows: 1000 ppm NO_x, 1000 ppm NH_3, 5 vol.% O_2, balance N_2 (200 mL min^{-1}), and $NO_x + O_2$ was composed of 1000 ppm NO + 5 vol.% O_2/N_2 or 500 ppm NO + 500 ppm NO_2 + 5 vol.% O_2/N_2. To investigate the reactions in detail, the $NO_x + O_2$ adsorbed species were set as background, and then NH_3 was introduced to the reaction cell. If the absorbance was negative, the corresponding surface species were consumed. Conversely, there were new species generated on the catalyst surface, if the absorbance was positive. All spectra were recorded by accumulating 100 scans with a resolution of 4 cm^{-1}.

2.3 Kinetic studies

The kinetic data for "standard SCR" and "fast SCR" were evaluated in a differential reactor with a 4 mm inner diameter at atmospheric pressure. About 5 mg of the catalyst diluted with 20 mg of SiC was loaded with a catalyst bed length of *ca.* 2 mm. Under different conditions, the NO_x conversion was kept less than 20% in the temperature range tested. To eliminate the effects of diffusion, a total gas flow rate of 500 mL min^{-1} and a particle size of 40–60 mesh were used. The

"standard SCR" gas mixture was composed of 500 ppm NO, 500 ppm NH_3, 5 vol.% O_2, and balance N_2, while the "fast SCR" gas mixture was composed of 250 ppm NO, 250 ppm NO_2, 500 ppm NH_3, 5 vol.% O_2, and balance N_2. The effluent gas was also analyzed using an online NEXUS 670-FTIR spectrometer as described above. NO_x reduction rates (mol g s^{-1}) were calculated as:

$$r_{NO_x} = X_{NO_x} Y_{NO_x,in} V_{gas}/m_{cat}$$

where X_{NO_x} is the NO_x conversion, $Y_{NO_x,in}$ is the NO_x molar fraction in the inlet gas, V_{gas} is the total flow rate in moles per second, and m_{cat} is the mass of the catalyst in grams.

3. Results and discussion

3.1 NH_3–SCR performance of the Cu–SSZ-13 catalyst under different NO_2/NO_x ratio conditions

The elemental content was analyzed using an inductively coupled plasma instrument (OPTMIA 2000DV) with a radial view of the plasma. There was 3.9% Cu content by weight remaining in the obtained catalyst, which was denoted as $Cu_{3.9}$–SSZ-13. The catalyst showed excellent NH_3–SCR performance under "standard SCR" conditions (Fig. S1†). In order to investigate the effect of NO_2, the activity tests were carried out from 150 to 550 °C with different NO_2/NO_x ratios in the feed gas, as shown in Fig. 1. In the low temperature range (≦200 °C), the NH_3–SCR performance of the catalyst became poorer with the increase of the NO_2 ratio. When the NO_2/NO_x ratio was changed from 0 to 0.5, the NO_x conversion decreased from 92.7% to 4.8% at 200 °C. During the activity test, a small amount of N_2O formed (less than 10 ppm) under "standard SCR" conditions, while under "fast SCR" conditions (NO_2/NO_x = 1/2), more N_2O was observed at temperatures higher than 250 °C, and the N_2O level increased significantly at temperatures from 200 to 250 °C, especially from 225 to 250 °C (Fig. S2†), implying the possible rapid decomposition of NH_4NO_3 which might be an important reaction intermediate for the SCR process at high temperatures. It was surprising that the improvement of NH_3–SCR activity under "fast SCR" reaction conditions was reversed, that is, NO_2 did not promote the activity of the Cu–SSZ-13 catalyst prepared by the one-pot-synthesis method but instead inhibited the reaction. This inhibitory effect was still distinct in the presence of 5% H_2O (Fig. S3†). Compared with the effect of NO_2 on metal oxide catalysts, transition metal-exchanged zeolite catalysts (such as Cu–ZSM-5 and Fe–ZSM-5) and even the Cu–SSZ-13 catalyst prepared by ion exchange method in previous reports, the conclusion was entirely opposite.[7,8,18,28,29] These observations suggested that the mechanism of the NH_3–SCR reaction over this catalyst was different, and more research is needed to investigate the true reason for the inhibitory effect of NO_2 on the NH_3–SCR reaction.

3.2 NH_3 adsorption

In situ DRIFTS spectra were collected to characterize the surface species during NH_3 adsorption on the $Cu_{3.9}$–SSZ-13 catalyst at 120 °C for 0.5 h, followed by a N_2 purge for 0.5 h. As shown in Fig. 2, strong IR bands at 1458 and 1621 cm^{-1} were observed. The band at 1458 cm^{-1} was assigned to NH_4^+ species adsorbed on the Brønsted acid sites, whereas the band at 1621 cm^{-1} was due to NH_3 coordinately linked to the Lewis acid sites.[12] There were four bands in the range from 3100 cm^{-1} to 3400 cm^{-1}, which were assigned to N–H stretching vibrations. In detail, the band at 3178 cm^{-1} was due to NH_3 adsorbed on Cu species. The bands at 3270 and 3332 cm^{-1} were attributed to NH_4^+ species, and the band at 3384 cm^{-1} was assigned to NH_3 molecules.[30–32] Meanwhile, the negative bands at 3567, 3602, 3654 and 3745 cm^{-1} were assigned to OH vibrations, corresponding to the Brønsted acid sites.[32–35] The NH_3 adsorbed species observed on the Cu–SSZ-13 catalyst prepared by the one-pot-synthesis method were similar to those seen on other Cu–CHA catalysts.

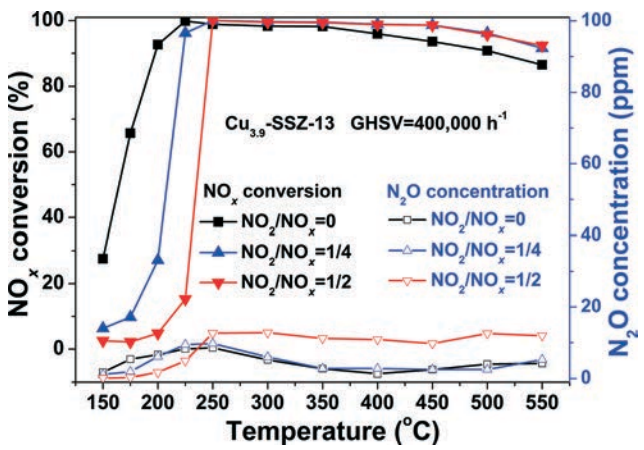

Fig. 1 NH_3–SCR performance of the $Cu_{3.9}$–SSZ-13 catalyst under different reaction conditions.

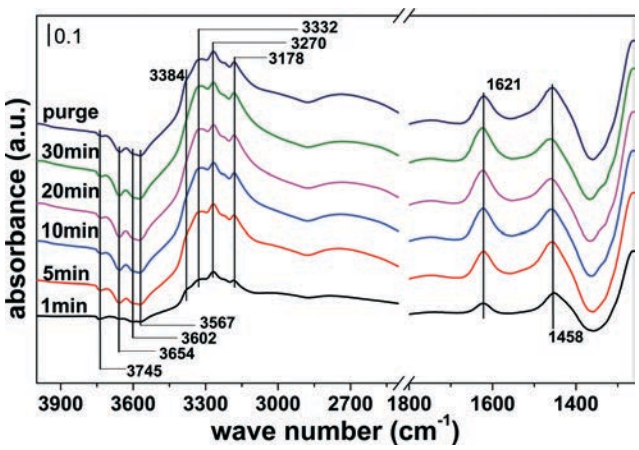

Fig. 2 *In situ* DRIFT spectra of species on the $Cu_{3.9}$–SSZ-13 catalyst during exposure to NH_3 at 120 °C.

3.3 NO_x adsorption

In order to identify the adsorbed NO_x species on the Cu–SSZ-13 catalyst and further investigate the difference caused by different NO_x sources, the sample was exposed to NO + O_2 or NO_2 + O_2 for 0.5 h and then purged in N_2 for 0.5 h. When the $Cu_{3.9}$–SSZ-13 catalyst was exposed to NO + O_2, three types of nitrate species were mainly observed, as shown in Fig. 3(a). They were assigned to monodentate nitrates (1504 cm^{-1}), bidentate nitrates (1573 and 1596 cm^{-1}) and bridging nitrates (1631 cm^{-1}).[36–40] All nitrate species formed simultaneously as soon as NO_x was introduced to the catalyst, indicating the good oxidation ability of the catalyst. When the sample was exposed to NO_2 + O_2, the adsorption progress was totally different, as shown in Fig. 3(b). Only bridging nitrates (1631 cm^{-1}) were formed on the catalyst surface in the first 4 min. Then, monodentate nitrates (1502 cm^{-1}) and bidentate nitrates (1575 and 1598 cm^{-1}) formed gradually. Only a small amount of nitrate species formed in 5 min using NO_2 + O_2, while much more nitrate species formed under the same conditions with NO + O_2. Thus, it was apparent that the formation speed of nitrate species was much slower when NO was replaced by NO_2 in the feed gas.

3.4 *In situ* DRIFTS experiments under "standard SCR" and "fast SCR" conditions

The *in situ* DRIFTS experiments were carried out to determine the species on the catalyst surface under real NH_3–SCR reaction conditions at 120 °C. The reaction time was controlled at 0.5 h, and the spectra were collected throughout. The stable surface species under different reaction conditions are shown in Fig. 4. When the NH_3–SCR reaction was conducted under "standard SCR" conditions, typical bands at 1479, 1620, 2825, 3062, 3186, 3270 and 3327 cm^{-1} were observed (Fig. 4(a)). According to the peak assignments described above, the peaks at 1620, 3186, 3270 and 3327 cm^{-1} were assigned to NH_3 adsorbed species, and the formation of a peak at 1479 cm^{-1} should be due to the combination of

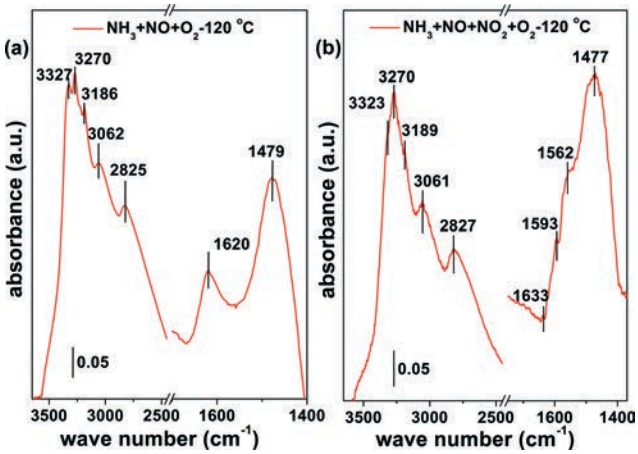

Fig. 4 *In situ* DRIFT spectra of stable species on the $Cu_{3.9}$–SSZ-13 catalyst under "standard SCR" conditions (a) and "fast SCR" conditions (b) at 120 °C.

NH_3 species at 1458 cm^{-1} and some nitrate species at 1504 cm^{-1}. In line with previous studies, it was supposed that peaks at 2825 and 3062 cm^{-1} could be assigned to NH_4^+ from NH_4NO_3.[41,42] Surface NH_4NO_3 species could participate in the NH_3–SCR reaction, following the equations: $NH_4NO_3 + NO \rightarrow NH_4NO_2 + NO_2$, $NH_4NO_2 \rightarrow N_2 + H_2O$.[43–45]

In order to confirm the assignment of peaks at 2825 and 3062 cm^{-1}, the *in situ* DRIFTS experiment was carried out to record the reactions between NO and the $Cu_{3.9}$–SSZ-13 catalyst (*ca.* 2 wt% NH_4NO_3 loaded on the surface). Because the spectrum of the catalyst loaded with NH_4NO_3 was set as the background, the negative peaks at 3270, 3041, 2832 and 1446 cm^{-1} should be assigned to NH_4^+ from NH_4NO_3 (Fig. 5). According to the nitrate species assignments above (Fig. 3), the positive peaks in the range from 1500 to 1700 cm^{-1} were attributed to the formation of new nitrate species. Thus, on the basis of the results in Fig. 2 and 5, it was concluded that NH_3 adsorbed species and a small amount of NH_4NO_3 formed on the catalyst surface under "standard SCR" conditions (Fig. 4(a)).

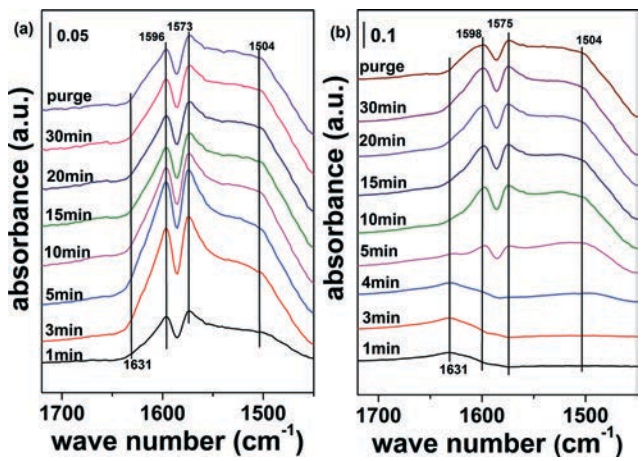

Fig. 3 *In situ* DRIFT spectra of species on the $Cu_{3.9}$–SSZ-13 catalyst during exposure to NO + O_2 (a) and NO_2 + O_2 (b) at 120 °C.

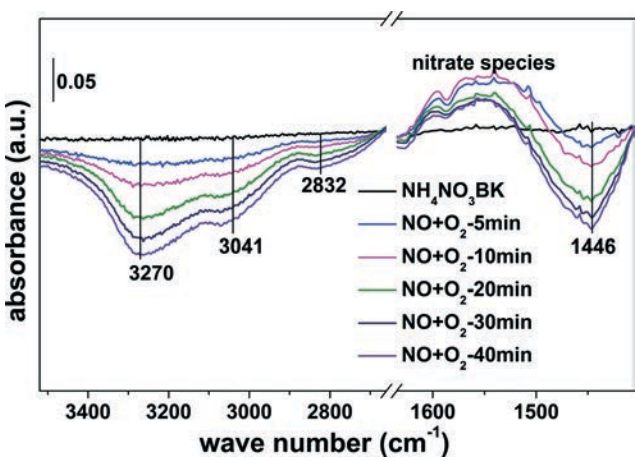

Fig. 5 Reduction of NH_4NO_3 loaded on the $Cu_{3.9}$–SSZ-13 catalyst by NO and O_2 at 120 °C.

The stable species on the catalyst surface under "fast SCR" reaction conditions were also recorded, as shown in Fig. 4(b). The peaks at 3323, 3189 and 3270 cm^{-1} indicated the adsorption of NH_3 species, and the peaks at 2827, 3061 and 3270 cm^{-1} proved that NH_4NO_3 was also deposited on the catalyst surface under these conditions. Compared with the results under "standard SCR" conditions (Fig. 4(a)), the intensity of the peak at 3270 cm^{-1} was higher, which should be due to the larger amount of NH_4NO_3 on the surface. More notably, a much larger amount of nitrate species was observed in the low wavenumber range (such as peaks at 1562, 1593 and 1633 cm^{-1}). All of these results proved that more NH_4NO_3 accumulated on the catalyst surface under "fast SCR" than under "standard SCR" conditions. Because NH_4NO_3 could block the pores and deactivate the active sites of the $Cu_{3.9}$–SSZ-13 catalyst, it was adverse for the deNO_x process. Therefore, the much greater amount of NH_4NO_3 deposited on the catalyst surface was the main reason for the NO_2 inhibitory effect on NH_3–SCR reaction in the low temperature range.

3.5 Reactions between pre-adsorbed species of NO_x and NH_3

In this study, the reactions between pre-adsorbed species of NO_x and NH_3 at 120 °C were chosen to represent the reactions in the low temperature range (Fig. 6). Because similar nitrate species were formed on the catalyst surface, regardless of whether NO + O_2 or NO_2 + O_2 contacted the catalyst (Fig. 3), nitrate species from NO + O_2 were chosen to react with NH_3 in this section. As shown in Fig. 6(a), upon the introduction of a NH_3 flow, the nitrate species (negative peaks at 1504, 1571 and 1596 cm^{-1}) decreased quickly with reaction time, especially in the first 10 min. New species (positive peaks at 1625 and 1458 cm^{-1}) could also be detected, which were caused by NH_3 adsorbed on the Lewis acid sites that were now free of nitrates and Brønsted acid sites, respectively. At the end of the reaction (shown in Fig. 6(b)), the stable species (3318, 3270, 3184, 3060, 2831, 1620 and 1471 cm^{-1}) were observed on the catalyst surface.

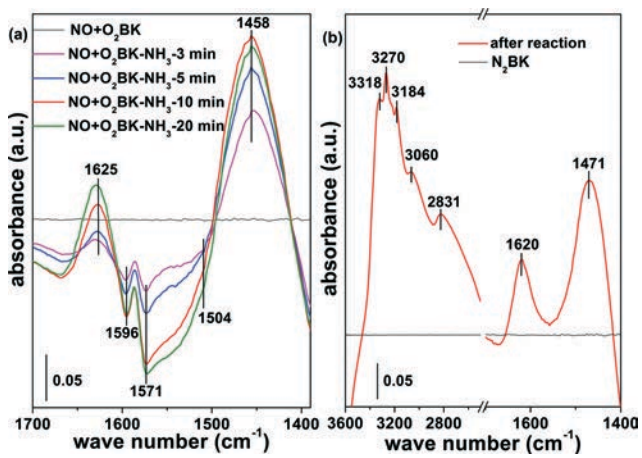

Fig. 6 Reactions between pre-adsorbed nitrate species and NH_3 at 120 °C on the $Cu_{3.9}$–SSZ-13 catalyst: (a) the reaction process recorded with nitrate species as the background; (b) the stable species maintained on the catalyst surface with N_2 as the background.

Clearly, the species were similar to those existing under "standard SCR" conditions (Fig. 4(a)), indicating that the reactions between nitrate species and gaseous NH_3 played an important role in the NH_3–SCR reaction for the Cu–SSZ-13 catalyst.

Grossale *et al.* reported that NH_3 could react with nitrate species on the surface of Fe–SZM-5 directly at temperatures higher than 220 °C, according to the following equation: $5NH_3 + 3HNO_3 \rightarrow 4N_2 + 9H_2O$.[15] The results in this study proved that the reaction could occur at a high rate at a much lower temperature (120 °C) over the Cu–SSZ-13 catalyst. Therefore, if NO_x could come in contact with the Cu sites and then form nitrate species efficiently, they could be consumed by NH_3 rapidly.

3.6 Kinetic diameter of NO_2 and the effect on NH_3–SCR reaction

The kinetic diameters of molecules play a very important role in predicting their diffusion and adsorption into zeolites, and they are obtained commonly from experimental data. However, the corresponding data are lacking for NO_2. Liu reported one method to estimate the average diameter of a molecule which is thought to be similar to the molecular kinetic diameter, giving a kinetic diameter for NO_2 in the range from 0.401 to 0.502 nm.[46] A space-filling model (CPK model) has also been used to calculate the kinetic diameter of molecules. Considering the uncertainty of the CPK model, we further calibrated the cross-sectional area using the model and experimental values of Ar, Kr, Xe, N_2, H_2O, CH_3OH, C_2H_6, C_6H_6, and CO_2.[47] The calibrated cross-sectional area of NO_2 was 0.206 nm^2. Thus, the kinetic diameter of NO_2 could be estimated as 0.512 nm. These two results indicate that the kinetic diameter of NO_2 was larger than 0.38 nm. Thus, different from NO with a kinetic diameter of 0.32 nm, the speed for NO_2 to enter the Cu–CHA pores and form nitrate species was much slower, as shown in Fig. 3(b). If some NO_2 molecules could not form nitrate species on the Cu sites efficiently and react with NH_3, they could combine with NH_4^+ on the other sites to form NH_4NO_3. The formation of NH_4NO_3 resulting from the reaction between nitrate species and NH_4^+ was very fast, but its consumption rate was much slower over the $Cu_{3.9}$–SSZ-13 catalyst (Fig. S4†). Ciardelli reported that NH_4NO_3 is an important intermediate in the "fast SCR" reaction, and the reaction between NH_4NO_3 and NO is the rate-determining step of the reaction at low temperatures. If the formation of NH_4NO_3 was faster than its decomposition, the "fast SCR" phenomenon would not be obvious.[2] Unfortunately, less NO could be used for its decomposition under "fast SCR" reaction conditions. Thus, much NH_4NO_3 accumulated on the catalyst surface under "fast SCR" reaction conditions, and active sites were blocked until NH_4NO_3 could be decomposed at a higher temperature. Therefore, the key step for the NH_3–SCR reaction over the Cu–SSZ-13 catalyst in the low temperature range was the formation of nitrate on the Cu sites. Increasing the NO_2 ratio directly in the feed gas was not an effective way to improve the NH_3–SCR performance of the Cu–SSZ-13 catalyst prepared by the one-pot-synthesis method.

3.7 Kinetic studies

In order to further prove the conclusions gained from the *in situ* DRIFTS results, we carried out some kinetic studies. The apparent activation energy (E_a) for NH_3–SCR on the $Cu_{3.9}$–SSZ-13 catalyst was estimated using the data obtained in the temperature range where NO_x conversion increased rapidly. When the NO_2/NO_x ratio was 0 or 1/2 in the feed gas, the tested temperature range was set at 160–200 °C or 210–250 °C, respectively. Based on the Arrhenius plot of the rate (R) *versus* inverse temperature (Fig. 7) at different NO_2/NO_x ratios, E_a was determined to be ~60 and ~89 kJ mol^{-1} for NO_2/NO_x = 0 and NO_2/NO_x = 1/2, respectively. Therefore, E_a of "standard SCR" was much lower than that of "fast SCR". The higher performance of "standard SCR" over the Cu–SSZ-13 catalyst correlated well with its lower activation barrier. The presence of NO_2 in the feed gas increased the apparent activation energy, thereby decreasing the activity of NO_x reduction.

Based on the Arrhenius plot of the rate (R) *versus* inverse temperature (Fig. 8) for NO and NO_2 when the NO_2/NO_x ratio was 1/2, the apparent activation energy was determined to be ~63 and ~110 kJ mol^{-1}, respectively. Since the reaction between NO and NH_3 showed lower E_a and higher reaction activity than the reaction between NO_2 and NH_3, it is reasonable to conclude that the N_2 formation mainly came from the reaction between NO and NH_3 under "fast SCR" conditions.

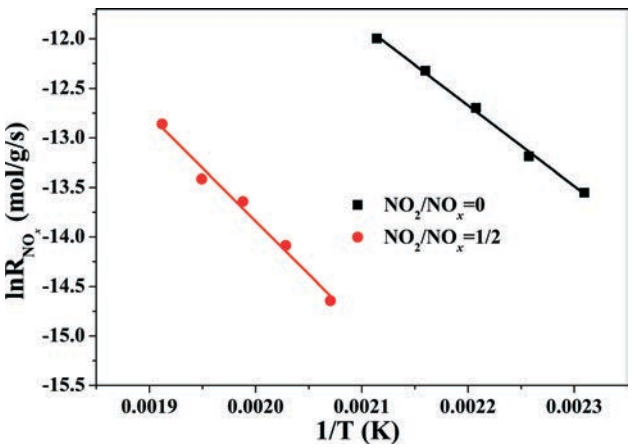

Fig. 7 Arrhenius plots of rate (R) of NO_x reduction *versus* inverse temperature under different NO_2/NO_x ratio conditions.

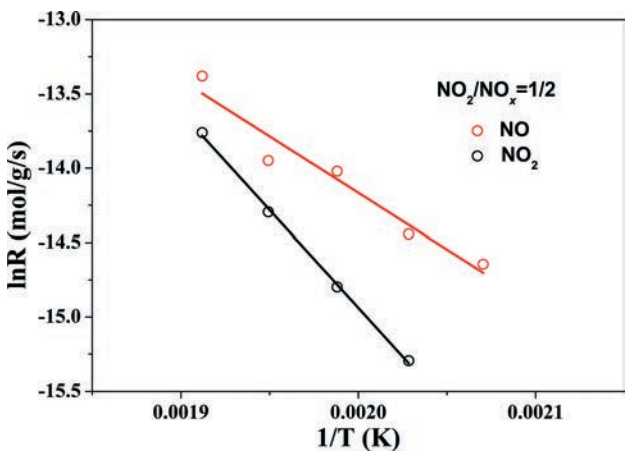

Fig. 8 Arrhenius plots of rate (R) *versus* inverse temperature of NO and NO_2 reduction when the NO_2/NO_x ratio was 1/2.

4. Conclusions

The $Cu_{3.9}$–SSZ-13 catalyst prepared by the one-pot-synthesis method exhibited excellent NH_3–SCR activity under "standard SCR" conditions. However, poorer SCR performance was observed in the low temperature range with the increase of the NO_2 concentration in the feed gas. The results of *in situ* DRIFTS experiments indicate that the inhibitory effect was caused by NH_4NO_3 deposition. The reactions between nitrate species and gaseous NH_3 played an important role in the NH_3–SCR reaction at low temperatures for the catalyst. Thus, the key step of the reaction was the formation of nitrate on the Cu sites. However, because the kinetic diameter of NO_2 was larger than the pores of the CHA structure, some NO_2 could not form nitrate on the Cu sites efficiently to react with NH_3 but combined with NH_4^+ on the Brønsted acid sites to form NH_4NO_3. The consumption rate of NH_4NO_3 by NO was slower than its formation under "fast SCR" conditions, resulting in much accumulated NH_4NO_3 on the catalyst surface blocking active sites. The results of kinetic studies indicate that the apparent activation energy was high when NO_2 was present in the feed gas, and the reaction between NO and NH_3 was dominant under "fast SCR" conditions.

Acknowledgements

This work was financially supported by the National Natural Science Foundation of China (51278486) and the National High Technology Research and Development Program of China (2013AA065301). The authors would also like to give thanks for the help from Dr. Yongchun Liu in calculating the kinetic diameter of NO_2 and Hua Deng for assignments of nitrate species.

Notes and references

1 B. Sandro, K. Oliver, T. Arno and A. Roderik, *Catal. Rev. Sci. Eng.*, 2008, **50**, 492–531.
2 C. Ciardelli, I. Nova, E. Tronconi, D. Chatterjee and B. Bandl-Konrad, *Chem. Commun.*, 2004, 2718–2719.
3 M. Moliner, C. Franch, E. Palomares, M. Grill and A. Corma, *Chem. Commun.*, 2012, **48**, 8264–8266.
4 J. H. Kwak, R. G. Tonkyn, D. H. Kim, J. Szanyi and C. H. F. Peden, *J. Catal.*, 2010, **275**, 187–190.
5 L. Wang, W. Li, G. Qi and D. Weng, *J. Catal.*, 2012, **289**, 21–29.
6 F. Liu, W. Shan, X. Shi and H. He, *Prog. Chem.*, 2012, **24**, 445–455.
7 H. Sjövall, R. J. Blint and L. Olsson, *Appl. Catal., B*, 2009, **92**, 138–153.
8 A. Grossale, I. Nova, E. Tronconi, D. Chatterjee and M. Weibel, *Top. Catal.*, 2009, **52**, 1837–1841.

9 A. Grossale, I. Nova, E. Tronconi, D. Chatterjee and M. Weibel, *J. Catal.*, 2008, **256**, 312–322.
10 X. Shi, F. Liu, L. Xie, W. Shan and H. He, *Environ. Sci. Technol.*, 2013, **47**, 3293–3298.
11 C. Ciardelli, I. Nova, E. Tronconi, D. Chatterjee, B. Bandl-Konrad, M. Weibel and B. Krutzsch, *Appl. Catal., B*, 2007, **70**, 80–90.
12 R. Q. Long and R. T. Yang, *J. Catal.*, 2002, **207**, 224–231.
13 P. Forzatti, L. Lietti, I. Nova and E. Tronconi, *Catal. Today*, 2010, **151**, 202–211.
14 X. Tang, J. Li, L. Sun and J. Hao, *Appl. Catal., B*, 2010, **99**, 156–162.
15 A. Grossale, I. Nova and E. Tronconi, *Catal. Lett.*, 2009, **130**, 525–531.
16 T. C. Brüggemann, D. G. Vlachos and F. J. Keil, *J. Catal.*, 2011, **283**, 178–191.
17 R. Martínez-Franco, M. Moliner, C. Franch, A. Kustov and A. Corma, *Appl. Catal., B*, 2012, **127**, 273–280.
18 J. H. Kwak, D. Tran, S. D. Burton, J. Szanyi, J. H. Lee and C. H. F. Peden, *J. Catal.*, 2012, **287**, 203–209.
19 L. Ma, Y. Cheng, G. Cavataio, R. W. McCabe, L. Fu and J. Li, *Chem. Eng. J.*, 2013, **225**, 323–330.
20 Q. Ye, L. Wang and R. T. Yang, *Appl. Catal., A*, 2012, **427–428**, 24–34.
21 D. W. Fickel, D. A. Elizabeth, J. A. Lauterbach and R. F. Lobo, *Appl. Catal., B*, 2011, **102**, 441–448.
22 J. H. Kwak, D. Tran, J. Szanyi, C. H. F. Peden and J. H. Lee, *Catal. Lett.*, 2012, **142**, 295–301.
23 H. Zhu, J. H. Kwak, C. H. F. Peden and J. Szanyi, *Catal. Today*, 2012, **205**, 16–23.
24 J. H. Kwak, J. H. Lee, S. D. Burton, A. S. Lipton, C. H. Peden and J. Szanyi, *Angew. Chem., Int. Ed.*, 2013, **52**, 9985–9989.
25 U. Deka, I. Lezcano-Gonzalez, S. J. Warrender, A. L. Picone, P. A. Wright, B. M. Weckhuysen and A. M. Beale, *Microporous Mesoporous Mater.*, 2013, **166**, 144–152.
26 L. Ren, L. Zhu, C. Yang, Y. Chen, Q. Sun, H. Zhang, C. Li, F. Nawaz, X. Meng and F.-S. Xiao, *Chem. Commun.*, 2011, **47**, 9789–9791.
27 L. Xie, F. Liu, L. Ren, X. Shi, F.-S. Xiao and H. He, *Environ. Sci. Technol.*, 2014, **48**(1), 566–572.
28 W. Shan, F. Liu, H. He, X. Shi and C. Zhang, *Chem. Commun.*, 2011, **47**, 8046–8048.
29 X. Wang, A. Shi, Y. Duan, J. Wang and M. Shen, *Catal. Sci. Technol.*, 2012, **2**, 1386–1395.
30 H. Sjövall, E. Fridell, R. J. Blint and L. Olsson, *Top. Catal.*, 2007, **42–43**, 113–117.
31 G. V. A. Martins, G. Berlier, C. Bisio, S. Coluccia, H. O. Pastore and L. Marchese, *J. Phys. Chem. C*, 2008, **112**, 7193–7200.
32 D. Wang, L. Zhang, K. Kamasamudram and W. S. Epling, *ACS Catal.*, 2013, **3**, 871–881.
33 B. Coq, G. Delahay, R. Durand, D. Berthomieu and E. Ayala-Villagomez, *J. Phys. Chem. B*, 2004, **108**, 11062–11068.
34 A. Mike, M. Olivier, B. Philippe and D. Marco, *J. Catal.*, 2010, **271**, 1–11.
35 J. Valyont and W. K. Hall, *J. Phys. Chem.*, 1993, **97**, 7054–7060.
36 M. Rivallan, G. Ricchiardi, S. Bordiga and A. Zecchina, *J. Catal.*, 2009, **264**, 104–116.
37 F. Liu and H. He, *Catal. Today*, 2010, **153**, 70–76.
38 L. Castoldi, R. Bonzi, L. Lietti, P. Forzatti, S. Morandi, G. Ghiotti and S. Dzwigaj, *J. Catal.*, 2011, **282**, 128–144.
39 K. I. Hadjiivanov, *Catal. Rev. Sci. Eng.*, 2000, **42**, 71–144.
40 E. Ivanova, K. Hadjiivanov, D. Klissurski, M. Bevilacqua, T. Armaroli and G. Busca, *Microporous Mesoporous Mater.*, 2001, **46**, 299–309.
41 M. Irene, M. Olivier, B. Philippe, D. Marco and J. Xavier, *Appl. Catal., B*, 2012, **113–114**, 52–60.
42 J. Eng and C. H. Bartholomew, *J. Catal.*, 1997, **171**, 27–44.
43 A. Grossale, I. Nova and E. Tronconi, *J. Catal.*, 2009, **265**, 141–147.
44 M. Li, Y. Yeom, E. Weitz and W. M. H. Sachtler, *Catal. Lett.*, 2006, **112**, 129–132.
45 X. Yang, Z. Wu, M. Moses-Debusk, D. R. Mullins, S. M. Mahurin, R. A. Geiger, M. Kidder and C. K. Narula, *J. Phys. Chem. C*, 2012, **116**, 23322–23331.
46 Y. Liu and Z. Gao, *Shiyou Xuebao, Shiyou Jiagong*, 1996, **12**, 35–39.
47 Y. Liu, Q. Ma and H. He, *Environ. Sci. Technol.*, 2012, **46**, 11112–11118.

